ACS APPLIED MATERIALS & INTERFACES

Research Article

www.acsami.org

A New Metal-Free Carbon Hybrid for Enhanced Photocatalysis

Hongqi Sun,*[,†] Guanliang Zhou,[†] Yuxian Wang,[†] Alexandra Suvorova,[‡] and Shaobin Wang*[,†]

[†]Department of Chemical Engineering and CRC for Contamination Assessment and Remediation of the Environment (CRC CARE), Curtin University, GPO Box U1987, Perth, Western Australia 6845, Australia

[‡]Centre for Microscopy, Characterisation and Analysis, The University of Western Australia, Crawley, Western Australia 6009, Australia

Supporting Information

ABSTRACT: Carbon nitride (C_3N_4) is a layered, stable, and polymeric metal-free material that has been discovered as a visible-light-response photocatalyst. Owing to C_3N_4 having a higher conduction band position, most previous studies have been focused on its reduction capability for solar fuel production, such as hydrogen generation from water splitting or hydrocarbon production from CO_2. However, photooxidation ability of g-C_3N_4 is weak and has been less explored, especially for decomposition of chemically stable phenolics. Carbon spheres prepared by a hydrothermal carbonization of glucose have been widely applied as a support material or template due to their interesting physicochemical properties and the functional groups on the reactive surface. This study demonstrated that growth of carbon nanospheres onto g-C_3N_4 (CN-CS) can significantly increase the photooxidation ability (to about 4.79 times higher than that of pristine g-C_3N_4) in phenol degradation under artificial sunlight irradiations. The crystal structure, optical property, morphology, surface groups, recombination rate of electron/hole pairs, and thermal stability of CN-CS were investigated by a variety of characterization techniques. This study contributes to the further promising applications of carbon nitride in metal-free catalysis.

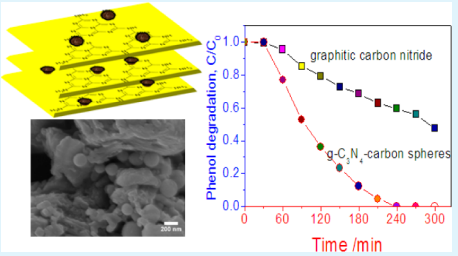

KEYWORDS: *carbon photocatalyst, metal-free catalysis, photodegradation, solar light, phenolics*

1. INTRODUCTION

Photocatalysis has achieved great success in environmental remediation, and a wide variety of photocatalyst materials, such as metal oxides,[1−3] metal sulfides,[4] and noble metals,[5] have been employed. High cost and dissolved metal ions of the photocatalyst materials have become the barriers to the wide application of photocatalysis. As fascinating alternatives to toxic or precious metals or their oxides, metal-free materials as green catalysts have demonstrated promising effectiveness in broad applications in chemical synthesis,[6,7] energy conversion and storage,[8,9] and environmental remediation.[10−12] For water purification, using metal-free materials as catalysts can exhibit more merit because they can completely prevent the potential toxic metal leaching and the associated secondary contamination.[13,14] Recently, graphene oxide (GO) was prepared by the modified Hummers' method and demonstrated as a promising photocatalyst for CO_2 conversion to methanol.[15] Carbon nanotube (CNT)-pillared reduced graphene oxide (RGO) composite materials exhibited an excellent visible light photocatalytic activity in degradation of a dye, rhodamine B, due to the unique porous structure and the exceptional electron transfer of graphene.[16] Carbon quantum dots (CQDs) can function as an effective near-infrared (NIR)-light-driven photocatalyst for the selective oxidation of benzyl alcohol to benzaldehyde, with 100% selectivity at 92% conversion.[17] Metal-free boron carbides ($B_{4.3}C$ and $B_{13}C_2$) were employed as efficient visible-light-responsive photocatalysts for H_2 evolution.[18] Moreover, metal-free elemental photocatalysts such as α-sulfur,[19] red phosphorus,[20] and β-rhombohedral boron[21] were also explored as visible-light-responsive photocatalysts.

As another promising metal-free photocatalyst, carbon nitride has also attracted considerable attention. Polymeric graphitic carbon nitride, g-C_3N_4, is the most stable allotrope, with a layered structure similar to graphene and has metal-free chemical compositions of C, N, and H. Due to the theoretical prediction of its unusual properties, promising applications of g-C_3N_4 in photocatalysis, heterogeneous catalysis and fuel cells have been demonstrated.[22−24] For the first time, Wang et al.[25] reported that g-C_3N_4 can produce hydrogen from water under visible-light irradiation in the presence of a sacrificial donor. Although the quantum efficiency was rather low, about 0.1% at irradiation 420−460 nm, the finding represented an important first step for the application of the metal-free, inexpensive, abundant polymer and stable semiconductor for solar energy conversion. The low activity was attributed to the high excitation energy and low charge mobility, low specific surface area, and the insufficient sunlight absorption.[26] To optimize the photocatalytic performance of g-C_3N_4, a variety of strategies have been employed, such as structural improvement (template[27,28] or template free[29]), coupling with other

Received: June 16, 2014
Accepted: September 12, 2014
Published: September 12, 2014

components (metal oxides,[30] monomer,[31] nanocarbons,[32] or dyes[33]), and introducing heteroatoms (metal[34] or nonmetal[35]). Figure 1 shows a comparison of band structures of TiO_2 and g-C_3N_4 and associated redox potentials for H_2 production, CO_2 reduction, and photooxidation.[36,37] Most studies have examined the photoreduction capabilities of modified g-C_3N_4, such as hydrogen evolution from water[25,27,33,38] or CO_2 conversion to hydrocarbon fuels.[39] On the other hand, the top energy level of valence band (VB) of g-C_3N_4 is at 1.4 V (vs NHE at pH = 7, compared to 2.7 V of TiO_2), resulting in a weak thermodynamical force (oxidative potential) for water oxidation and not enough for producing hydroxyl radicals.[31] Some efforts have been made to improve the photooxidation ability of g-C_3N_4. A porous g-C_3N_4 was synthesized by a facile template-free method to increase surface area and pore volume, and the prepared material showed an enhanced photocatalytic activity in methyl orange photodegradation.[40] It was reported that a novel carbon nitride with ordered and hollow structure was prepared from a cyanuric acid−melamine complex, and the new material showed a higher activity in photodegradation of rhodamine B than bulk material.[41] By incorporating electron-deficient pyromellitic dianhydride (PMDA) monomer into the network of g-C_3N_4, the valence band position was decreased to improve the photooxidation capability. The photocatalytic performances of g-C_3N_4−PMDA in water oxidation and degradation of methyl orange were significantly enhanced.[31] A urea precursor was used to prepare mesoporous g-C_3N_4 with silica as a hard template. It was found that the mesoporous g-C_3N_4 achieved 74% of phenol removal in 6 h, compared to bulk counterpart showing 20% phenol degradation in 6 h irradiation.[42] Cui et al.[43] prepared mesoporous g-C_3N_4 by thermal-induced polymerization of NH_4SCN using silica nanoparticles as the templates. Photodegradation of phenol or 4-chlorophenol was carried out on the mesoporous and nonporous g-C_3N_4, and only mesoporous samples were found to be effective for the organics removal. Chang et al.[44] prepared a novel mesoporous g-C_3N_4/BiOI heterojunction and found that it had an enhanced performance in degradation of bisphenol A (BPA) under visible light irradiations.

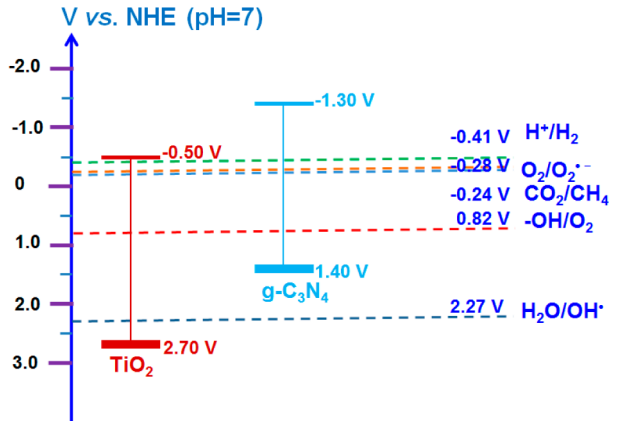

Figure 1. Schematic band structures of TiO_2 and g-C_3N_4 and typical redox potentials for photoreduction and photooxidation.[36,37]

Carbon spheres have attracted considerable research interests. Usually, hydrothermal treatment of carbon precursors at a high temperature range of 160−200 °C was used to prepare spherical carbon materials.[45,46] Sevilla and Fuertes[47] reported that the size-controlled carbonaceous colloids can be easily fabricated by the hydrothermal conditions ranging from 170 to 240 °C. Yao et al.[48] reported that carbon spheres would be formed at temperatures above 160 °C. Many applications of carbon spheres in catalyst supports, adsorbents, drug delivery systems, electrode materials, and templates for fabrication of core/shell or hollow structures have been reported.[49] Herein, for the first time, we report our finding that the carbon nanospheres can be a promising promoter for improving phenol photooxidation on polymeric carbon nitride with about 5-fold enhancement. The metal-free nanocomposite of g-C_3N_4 with carbon nanospheres (CN-CS) therefore demonstrated as a green material for sustainable remediation of aqueous organics driven by sunlight irradiations.

2. EXPERIMENTAL SECTION

2.1. Chemicals and Materials. Melamine (99.0%) was obtained from Aldrich and D-glucose (99.5%) was received from Sigma. 5,5-Dimethyl-1-pyrroline (DMPO, >99.0%) was obtained from Sigma-Aldrich. Ethanol (99.9%) was obtained from Chem Supply. All the chemicals were used as received without any purification.

2.2. Synthesis of g-C_3N_4/Carbon Nanospheres (CN-CS). The nanocomposites were synthesized by a thermal polycondensation of melamine to C_3N_4[50] and then followed by a hydrothermal carbonization of D-glucose.[51] In a typical synthesis, 5 g of melamine powders was put into a crucible with a loose cover and then heated in static air within a furnace at 500 °C for 2, 4, or 6 h. The heating rate was kept at 15 °C/min, and the furnace was naturally cooled to room temperature. The semiclosed system resulted in the polycondensation of melamine to g-C_3N_4 (CN). For preparation of the composite, 1.81 g of CN (prepared by calcination at 500 °C for 2 h) was mixed with 7.24 g of D-glucose in 80 mL of ultrapure water and magnetically stirred for 6 h. The mixed solution was then transferred to a Teflon-lined stainless steel autoclave (120 mL). The hydrothermal carbonization was conducted in an oven at 135, 150, and 180 °C for 3 h (or otherwise indicated). After cooling to room temperature, the obtained precipitates were filtrated and washed by ethanol/water for two cycles, followed by washing with ultrapure water. The obtained hybrid materials were then dried in an oven at 70 °C overnight. The prepared samples were then denoted as CN-CS-[temperature: 135, 150, or 180]-[duration: 1.5, 3, or 6 h]. For evaluation of the CN-CS composition, yield analysis was carried out. Due to the separation procedure and hydrolysis of 1.81 g of CN, 1.78, 1.77, and 1.75 g remained after hydrothermal treatment with pure water at 135 °C for 3 h, 150 °C for 3 h, and 180 °C for 3 h, respectively. In the CS formation, 0.056 and 0.326 g of CS was obtained at 180 °C for 3 and 6 h, respectively. In the preparation of CN-CS, the weights of CN-CS-135-3h, CN-CS-150-3h, CN-CS-180-3h and CN-CS-180-6h were 1.77, 1.78, 1.78, and 2.63 g, respectively. The CS weight percentages in CN-CS-135-3h, CN-CS-150-3h, and CN-CS-180-3h were calculated (referring to CN residue after hydrothermal treatment with water) to be 0%, 0.56%, and 1.69%, respectively.

2.3. Characterization of Materials. The crystalline structures of g-C_3N_4 and various CN-CS photocatalysts were analyzed by powder X-ray diffraction (XRD). The patterns were obtained on a Bruker D8-Advance X-ray diffractometer (Germany) with Cu Kα radiation (λ = 1.5418 Å). The Brunauer−Emmett−Teller (BET) surface area and pore size distribution were evaluated by nitrogen sorption at −196 °C using a Micromeritics Tristar 3000 apparatus. UV−visible diffuse reflectance spectra (UV−vis DRS) of samples were recorded on a JASCO V-670 spectrophotometer with an Ø 60 mm integrating sphere, and $BaSO_4$ as the reference material. Scanning electron microscopy (SEM), performed on a Zeiss Neon 40EsB FIBSEM, was used to evaluate the morphology, size, and textural information on the samples. Transmission electron microscopy (TEM) was carried out using a JEOL 3000F field emission TEM. Fourier transform infrared (FTIR) spectra were acquired on a Bruker instrument, using an ATR mode. Thermogravimetric analysis-differential scanning calorimetry (TGA-DSC) was carried out on a Mettler-Toledo Star system in air

flow at a heating rate of 10 °C/min. The photoluminescence (PL) spectra of the materials were acquired on a Varian Cary Eclipse spectrometer at an excitation wavelength of 330 nm.

2.4. Photodegradation of Phenol Solutions. The photocatalytic degradation of aqueous phenol was carried out in 1 L of Pyrex double-jacket reactor. A water bath connected with a pump was used to maintain the reaction temperature at 30 °C, and a magnetic stirrer was used to keep the photocatalyst dispersed homogeneously in the reaction solutions. In a typical run, 0.2 g of photocatalyst (1.0 g/L) was added into 200 mL of 20 ppm phenol solution and stirred for 30 min for adsorption−desorption equilibrium, and the first solution sample was taken. The light irradiation was immediately switched on after the first sampling. The irradiations were supplied by an MSR 575/2 metal halide lamp (575 W, Philips). The UV intensity ($315 < \lambda < 400$ nm) was measured to be 6.9 mW/cm^2 and the visible light intensity ($\lambda > 400$ nm) was 129.0 mW/cm^2. At each time interval, 1 mL of solution was withdrawn with a syringe and filtered through a 0.45 μm Millipore film into a high-performance liquid chromatography (HPLC) vial. The adsorption test was carried out in the same system without the irradiation on. The concentration of phenol was analyzed via HPLC (Varian, USA) with a UV detector set at $\lambda = 270$ nm. A C-18 column was used to separate the organics while the mobile phase of 30% CH_3CN and 70% water was flowing through the column at a flow rate of 1.0 mL/min. Electron paramagnetic resonance (EPR) experiments were performed on a Bruker EMX-E spectrometer (Germany) to analyze in situ generation of reactive radicals during the photocatalytic reaction. DMPO was applied to capture the produced radicals by activation of the photocatalyst under irradiations. The parameters for EPR analysis are centerfield, 3517 G; sweep width, 100 G; microwave frequency, 9.87 GHz; modulation frequency, 100 GHz; and power, 18.11 mW.

3. RESULTS AND DISCUSSION

3.1. Characterization of CN and CN-CS Samples. XRD was employed to monitor the crystal phase of the g-C_3N_4 via the polycondensation and the changes of crystal structures of CN-CS composites after the followed hydrothermal carbonization. Figure 2 shows the XRD patterns of g-C_3N_4 and its

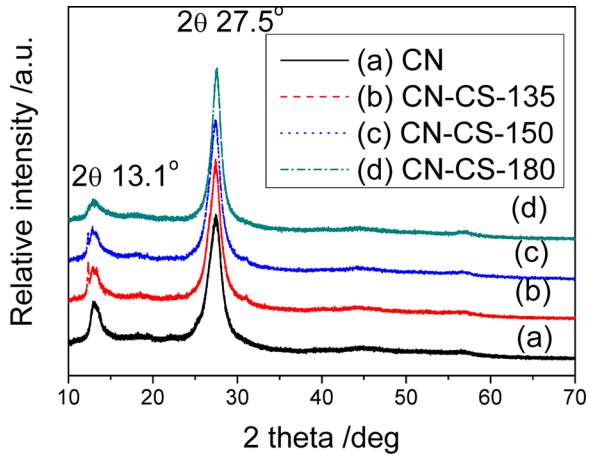

Figure 2. XRD patterns of different CN and CN-CS photocatalysts.

carbon sphere hybrids from the hydrothermal carbonization of glucose at different temperatures in 3-h duration. On the CN, a strong peak at 27.5° was observed, which was originated from the (002) interlayer reflection of a graphitic-like structure, corresponding to an interlayer distance of 0.324 nm.[38] Another XRD peak at 13.1° was also found, relating to in-plane repeated units and the (100) crystal plane. The interplanar distance was determined to be 0.676 nm, which was slightly smaller than the size of the tris-*s*-triazine unit (ca. 0.730 nm), possibly due to the presence of small tilt angularity in the structure.[52] The two characteristic peaks confirmed the transformation of graphitic structure from melamine via the polycondensation at 500 °C. Similar XRD patterns were obtained by Antonietti et al. in their studies on g-C_3N_4 nanoparticles[53] and mesoporous carbon nitrides.[54] Upon further hydrothermal treatment at 135 and 150 °C, the peaks at (002) plane moved to 27.4°, indicating the transformation to a slightly enlarged interlayer. Moreover, two new peaks at 12.3 and 31.1° appeared after hydrothermal carbonization of glucose, but their intensities decreased at higher temperature and almost disappeared at 180 °C. It was reported that hydrothermal treatment of g-C_3N_4 at above 110 °C would result in significant hydrolysis and generation of melem,[56] which is a product of thermal condensation of melamine (or urea and thiourea) before the formation of g-C_3N_4.[57] The new peaks in this study matched the characteristic peaks of melem very well. At a higher hydrothermal temperature, carbonization of glucose would first occur, and the intermediates/products then covered g-C_3N_4 particles and prevented the possible hydrolysis. That might be the reason that no vice peaks were observed at a higher hydrothermal temperature. The (100) peaks at ca. 13.1° became weaker at increased hydrothermal temperature. Figure S1 (Supporting Information) also shows XRD patterns of CN, CN-CS-180-3h, and CN-CS-180-6h. Compared with pure CN, the intensity of the (100) peak decreased after hydrothermal treatment with glucose. When the hydrothermal duration was prolonged, the intensity of the (100) peak also declined, suggesting that the crystal structure can be partially destroyed by the hydrothermal treatment.

The surface area, pore volume, and pore size of the composites and the reaction efficiencies are shown in Table 1. Figure S2 (Supporting Information) shows nitrogen sorption

Table 1. Surface Area, Pore Structure, and Reaction Rate Constants of the Materials

sample	S_{BET} ($m^2\ g^{-1}$)	V ($cm^3\ g^{-1}$)	pore radium (nm)	rate constant ($\times 10^{-3}\ min^{-1}$)
CN	6.0	0.029	13.3	2.46
CN-CS-135−3h	8.0	0.038	12.2	2.62
CN-CS-150−3h	7.0	0.026	9.0	9.84
CN-CS-180−3h	6.7	0.026	7.6	11.78
CN-CS-180−6h	2.7	0.008	6.3	2.03

isotherms and pore size distributions of CN and CN-CS samples. It can be found that the pristine g-C_3N_4 only has very low specific surface area (S_{BET}) of 6.0 m^2/g. Hydrothermal treatment at 135 °C would slightly increase the S_{BET}, which was decreased at the increasing temperature or prolonging duration. Associated with the low surface areas, very low pore volumes were observed for all the samples. Due to the formation of carbonaceous material, the pore radii continuously decreased with the hydrothermal treatment. Moreover, Barrett−Joyner−Halenda (BJH) pore size distributions showed that pure CN had a sharp peak (ca. 1.0 nm) of nanopore distribution. Hydrothermal treatment of CN at 135 and 150 °C produced bimodal nanopore distribution centered at ca. 1.0 and 2.2 nm, respectively. The bimodal distribution disappeared at a higher hydrothermal temperature of 180 °C. Taking XRD patterns into account, the latter nanopores at 2.2 nm were generated probably due to the hydrolysis of g-C_3N_4. It was also found that CN-CS-180-6h had a much lower S_{BET} and lower pore size, due

to the highest degree of carbonization of glucose under the hydrothermal condition and because the associated intermediates can block the porous structure of pure CN. SEM image and yield analysis also confirmed the largest amount of carbon spheres on the CN-CS-180-6h derived from the high degree of carbonization.

Figure 3 presents FTIR spectra of CN, CS-180-3h and CN-CS-180-3h. On CN, all the characteristic vibration modes

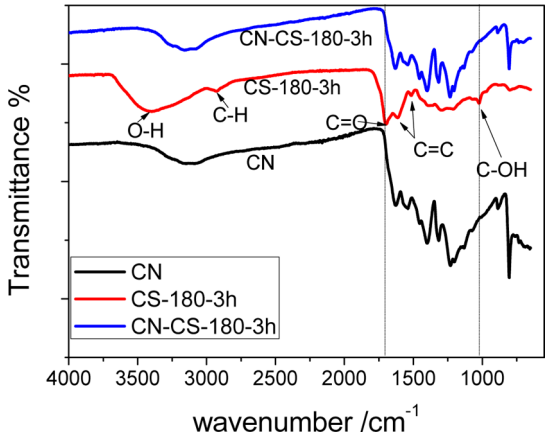

Figure 3. FTIR spectra of pure C_3N_4, CS-180-3h and CN-CS-180-3h.

relating to the typical g-C_3N_4 were observed, indicating the successful growth of carbon nitride.[33,57,58] The sharp peak at 805 cm^{-1} was considered to be the characteristic breathing mode of the triazine units. The strong bands at 1200−1650 cm^{-1} were assigned to the stretching vibration of the heptazine heterocyclic ring (C_6N_7). The peaks at 1317 and 1633 cm^{-1} were attributed to C−N and C═N stretching modes, respectively. The broad peak at 3000−3400 cm^{-1} was ascribed to the presence of NH or NH_2 groups, possibly due to the integral parts of the structure from the incomplete condensation.[59] In the spectrum of CS-180-3h, one broad OH peak at around 3400 cm^{-1} was observed. As the characteristic peaks of hydrothermal carbonization (HTC) materials, the peaks at 1700 and 1020 cm^{-1}, corresponding to C═O and C−OH, respectively, can be found, as suggested by Antonietti et al.[59] In the spectrum of CN-CS, the characteristic peaks of CS, however, were not clear. As shown in yield analysis, though, HTC at 180 °C for 3 h can produce CS; the yield was low, only at 0.768 g CS per 100 g glucose. The low content of CS on CN might lead to the similar spectrum of CN-CS to CN. Figure S3 (Supporting Information) shows FTIR spectra of CN-CS-150 samples. Yield analysis showed that no appreciable carbon spheres were produced at 150 °C; however, a longer duration would significantly increase the intensities of the peaks, indicating that hydrolysis of CN and carbonization of glucose occurred.

It was reported that the tri-*s*-triazine ring structure and the high-temperature condensation make g-C_3N_4 have a high thermal stability up to 600 °C.[22,43,56] Figure 4 shows TGA profiles of CN and CN-CS samples. CN was stable up to 510 °C, with a weight loss less than 1% at 510 °C. At higher temperatures, weight loss took place rapidly, corresponding to the decomposition of C−N bonds. Lee et al.[42] reported that a prepared g-C_3N_4 was stable up to 450 °C, which was from polymerization of urea at 550 °C. Zhang et al.[56] reported the stability up to 550 °C of the g-C_3N_4 sample prepared at 600 °C. It was indicated that the thermal stability is closely related to the condensation temperature. Figure 4B shows the exothermic peak of CN is centered at 694.9 °C, referring to the fast oxidation of the polymer-like material. The hydrothermal carbonization of glucose on the g-C_3N_4 was clearly shown in the TGA profiles. About 5% weight loss before 120 °C on four CN-CS samples was found due to desorption of water or ethanol from the washing processes. CN-CS-135-3h and CN-CS-150-3h were then stable until the temperature of 400 °C, while the onset temperature of CN-CS-180-3h and -6h were 253 and 184 °C, respectively. Similar to CN, weight loss occurred very fast at the above onset temperature. In the synthesis, upon hydrothermal carbonization, the glucose will form amorphous carbon as cores and hydrophilic surface. The lower onset temperature was ascribed to the lower temperature of the dehydration and densification of the amorphous carbon and the surface groups at 230−390 °C.[51,60] It was also found that the onset temperature decreased with increased hydrothermal temperature or prolonged duration, indicating more carbon nanospheres produced. Figure 4B shows that the exothermic peaks moved to lower temperature due to the hydrothermal carbonization. The peaks of CN-CS samples were broader than CN, indicating the combustion of different organic compounds. CN-CS-180-6h had a distinct exothermic peak at 317.6 °C due to the dehydration and densification of the larger amount of carbon nanospheres.[60]

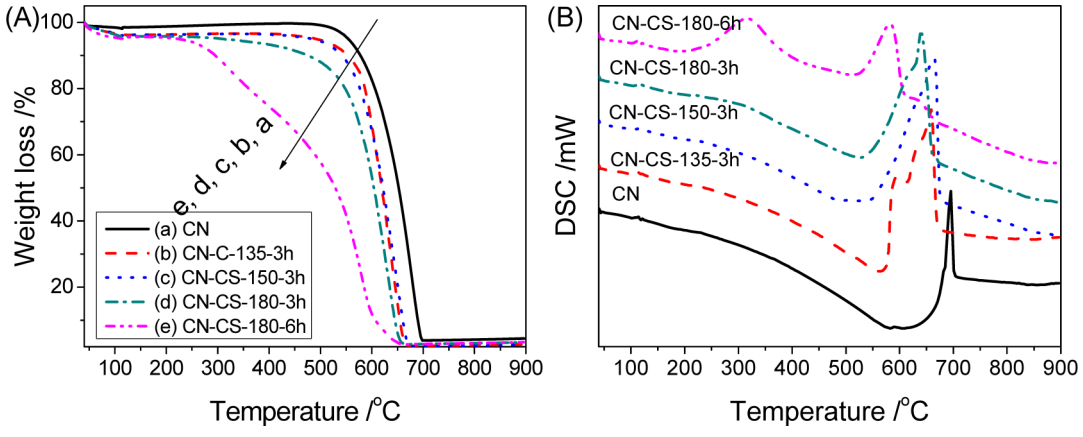

Figure 4. TGA profiles of CN and CN-CS photocatalysts (A) TG and (B) DSC.

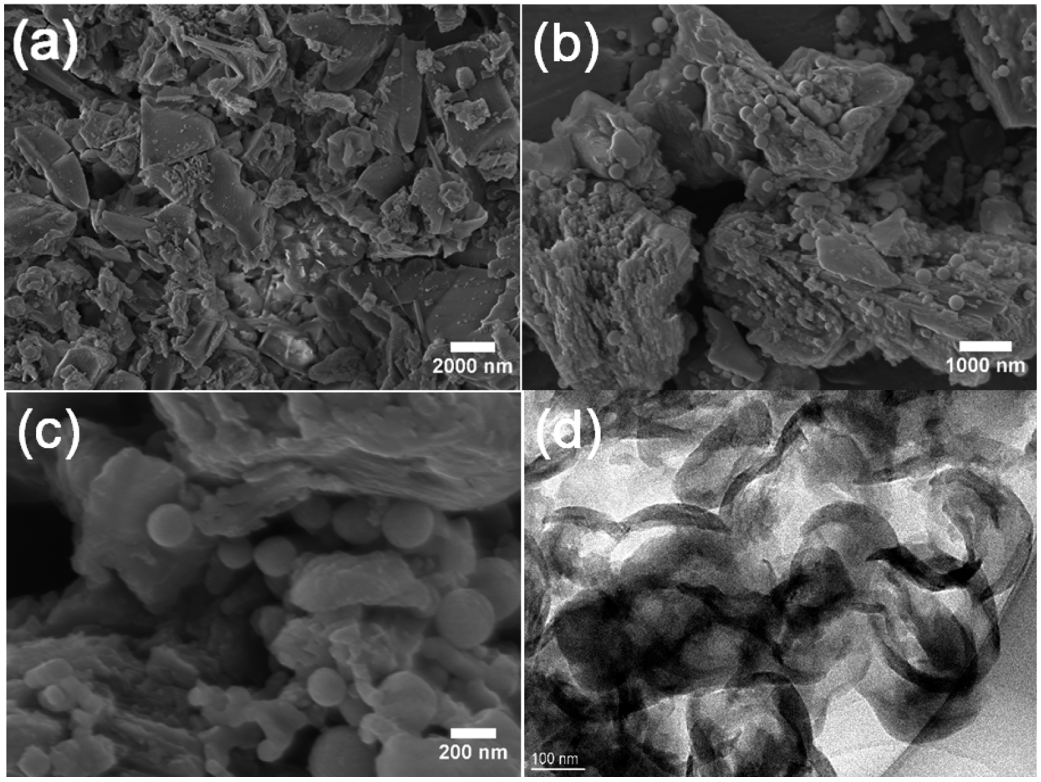

Figure 5. (a) SEM image of CN and (b) SEM image, (c) high-resolution SEM, and (d) TEM images of CN-CS-180-3h.

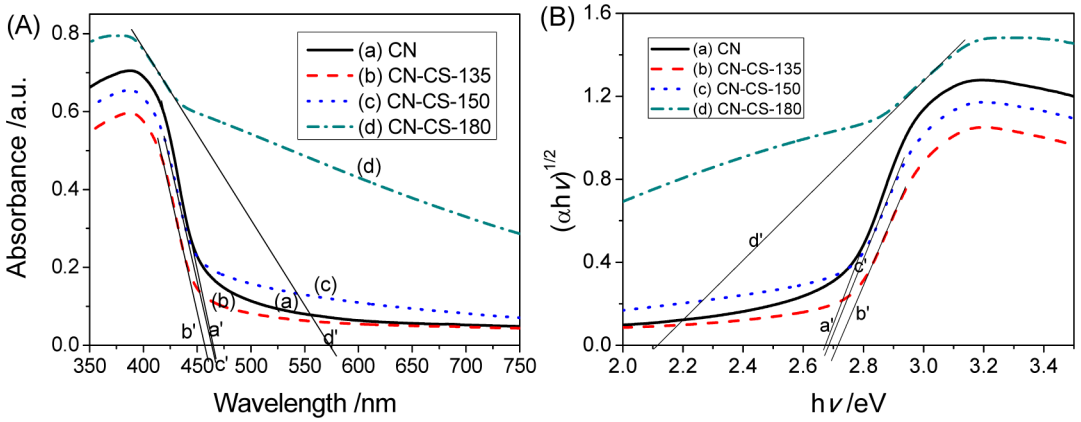

Figure 6. (A) UV−vis DRS and (B) evaluation of band gap energies by the Kubelka−Munk equations of CN and CN-CS photocatalysts.

The morphology of CN and the formation of carbon nanospheres via hydrothermal carbonization were studied by SEM imaging. Figure 5 shows the SEM images of CN, CN-CS-150-3h, and CN-CS-180-3h. Pristine CN in Figure 5a presented agglomeration structure with typical slate-like, stacked lamellar texture and sharp edges.[38,40] After hydrothermal treatment with glucose, the sharp edges became smooth, and the aggregation was mitigated. As a result, the layered structure is very stable. There are very limited studies that reported the effect of hydrothermal treatment on the structure of g-C_3N_4. Li et al.[61] suggested that hydrothermal treatment of g-C_3N_4 H_2O_2 would corrode the slate-like structure and produce hierarchical edges, which was attributed to the random oxidation by H_2O_2. Sano et al.[55] found that the bubble wall of carbon nitride is not stable and can be decomposed by alkaline solution in hydrothermal treatment. The observations indicated that hydrolysis of g-C_3N_4 might occur in hydrothermal treatments. In this study, the formation of carbon nanospheres was also associated with the hydrothermal treatment due to the presence of glucose. In the condition of 150 °C for 3 h, the carbon nanospheres were not generated as clearly shown in Figure S4 (Supporting Information). Increasing the hydrothermal temperature to 180 °C led to the formation of more carbon spheres, as shown in Figure 5b. High-resolution SEM image of CN-CS-180-3h is shown in Figure 5c. It was found that carbon nanospheres, at a size of 100−300 nm, were closely attached to g-C_3N_4. Some carbon nanospheres formed sandwich-like structure in the g-C_3N_4 stacked layers. TEM image of CN-CS is shown in Figure 5d, indicating the size of ca. 200 nm and the structure of hollow sphere. It was reported that the production of carbon spheres is strongly dependent on the hydrothermal conditions, such as temperature, duration, and concentration of glucose.[47,62] It was reported that carbon nanospheres were only able to be

obtained at above 160 °C from the precursor of glucose.[48] In this study, at the conditions of 150 °C for 3 h, not many nanospheres were produced, but they were produced at the same temperature for 6 h, as shown in Figure S4 (Supporting Information). Sun and Li[62] reported that the growth of carbon spheres follows the LaMer model, and no carbon spheres can be formed when a 0.5 M glucose solution was hydrothermally treated below 140 °C for less than 1 h. But before the formation of carbon spheres, some aromatic compounds and oligosaccharides can be formed, as evidenced by the color change to orange or red and increased viscosity during polymerization step. The formation of organic compounds onto g-C_3N_4 was already confirmed by XRD, FTIR, and TGA, as shown before. Meanwhile, when the conditions were changed to 180 °C for 6 h, carbon microspheres were generated (Figure S4, Supporting Information).

Optical property is very important for a photocatalyst, and it can enable us to evaluate the light absorption threshold and estimate the band gap energy. Figure 6A shows UV DRS of g-C_3N_4 and its composites. The pure graphitic carbon nitride has an absorption edge at about 465 nm, which is consistent with the reported value.[25] The samples of CN-CS-135 and CN-CS-150 showed blue-shift with absorption edges at 457 and 463 nm, respectively. The blue-shift is very common on modified g-C_3N_4 samples. Zhang et al.[63] reported that the optical absorption of g-C_3N_4 was blue-shifted from 481 to 424 nm after protonation by reactions with HCl. Liu et al.[35] observed the blue-shift of g-C_3N_4 after sulfur doping. Compared to bulk g-C_3N_4, an obvious blue shift was found on nanosheets prepared by thermal oxidation, and the blue-shift in wavelength of ~20 nm was attributed to the well-known quantum confinement effect.[38] Sano et al.[55] suggested that alkaline hydrothermal treatment of g-C_3N_4 can also lead to blue-shift, due to the decreased scattering factor. In this study, mass carbon spheres were not produced at the conditions of 135 or 150 °C for 3 h. Therefore, the blue-shift in wavelength below 10 nm on CN-CS-135 and CN-CS-150 might be ascribed to the structural changes from g-C_3N_4 hydrolysis, as reported by Sano et al.[55] When the hydrothermal temperature was further increased to 180 °C, the blue-shift disappeared and significant red-shift was observed due to the formation of carbon spheres that modified the composition of the photocatalysts. The absorption threshold was also increased to 573 nm. Figure S5 (Supporting Information) shows that the optical absorption was significantly changed after hydrothermal treatment for 6 h, due to the considerable production of carbon spheres as confirmed in SEM images. The band gap energies of semiconductor photocatalysts can be estimated by the Kubelka–Munk theory.[64] In this study, $(\alpha h\nu)^n$ (n = 1/2) versus $h\nu$ of the materials were plotted in Figure 6B. The band gap energies of CN, CN-CS-135, -150, and -180 were then determined to be 2.67, 2.71, 2.68, and 2.12 eV, respectively. The results showed that the band gap of pure CN was similar to previously reported values,[25] and after hydrothermal treatment, the band gap energies of CN-CS changed.

Optical properties reflect the absorption abilities of the photocatalysts to incoming photons in the irradiations, while the effective utilization of the photons in photocatalysis also relies on the separation rate of the produced electron/hole pairs activated by the photons. Figure 7 shows the PL spectra of pure g-C_3N_4 and CN-CS samples. Upon the excitation at 330 nm, the main emission peak of g-C_3N_4 was observed at around 450 nm, due to the band gap recombination of electron/hole pairs.[65] Pure g-C_3N_4 had a high recombination rate of photoinduced carriers, which was decreased by hydrothermal treatment at 135 or 150 °C. CN-CS-180 had a very low intensity of emission in PL spectrum, indicating a low recombination rate and high photocatalytic activity.[66]

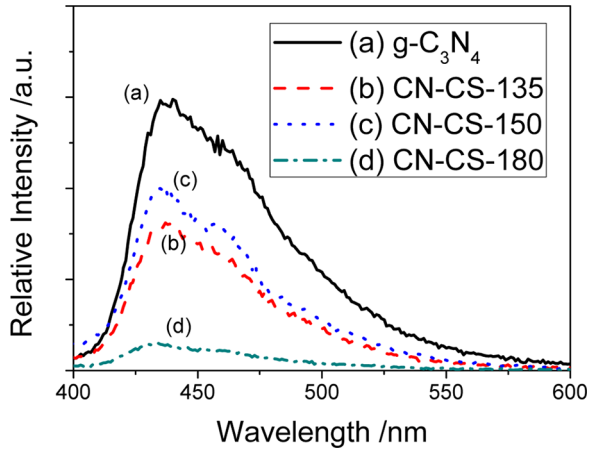

Figure 7. Photoluminescence (PL) spectra of CN and CN-CS samples.

3.2. Photodegradation of Phenol Solutions under Simulated Sunlight. The activities of CN and the effects of hydrothermal treatment and carbon spheres on the photodegradation efficiency were investigated by photocatalytic oxidation of phenol solutions under simulated sunlight irradiations. The polycondensation of melamine was conducted at 500 °C in varying period, and Figure 8A shows the effect of polycondensation duration on the photocatalytic activity of g-C_3N_4. The phenol removal at 30 min was from adsorption and was very minor, except for CN-500-6h, which had around 9% phenol adsorption. However, polycondensation duration did not produce significant effect on photocatalytic activity. Thus, CN-CS composite samples were prepared based on the CN synthesized at 500 °C for 2h. For adsorption tests without irradiations, CN-500-2h did not show significant removal of phenol without irradiations in 3 h. Figure 8B shows the effect of hydrothermal carbonization of carbon spheres onto CN on the photodegradation of phenol solutions. The adsorption was below 5% on all the samples. Pure CS-180-3h can only produce about 4% phenol removal. For photodegradation on CN, the photoreaction in 270 min was able to decompose 47.8% of 20 ppm phenol. CN-CS-135-3h had a slightly higher activity than pristine CN, providing 56.5% phenol removal at photodegradation time of 270 min. It was interesting to find that the CN-CS samples treated at 150 and 180 °C showed very high activities. CN-CS-150-3h made 20 ppm phenol completely decomposed after 270 min, while CN-CS-180-3h was able to degrade all phenol after 210 min. Yield analysis and SEM images showed that there were no considerable carbon spheres formed on CN-CS-150-3h, but crystal- and microstructure were modified after the hydrothermal treatment. PL spectra also suggested that the separation efficiency of photo-induced electron/hole pairs was improved. Structural changes increased the separation rate of carriers, and the modified surface feature might work together to contribute to the improved activity of CN-CS-150-3h. Once the hydrothermal temperature was increased to 180 °C, a significant amount of carbon spheres were produced on CN-CS-180-3h, leading to the lower band gap energy and significant enhancement of carrier separation.

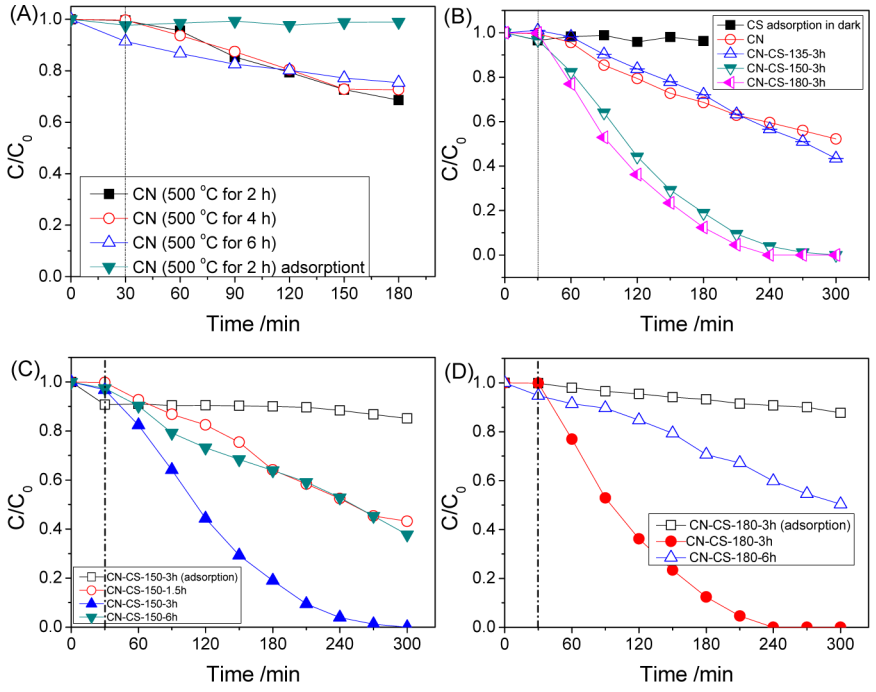

Figure 8. Photodegradation of phenol solutions; (A) effect of polycondensation duration, (B) effect of hydrothermal temperature, (C) effect of hydrothermal duration at 150 °C, and (D) effect of hydrothermal duration at 180 °C.

Therefore, CN-CS-180-3h showed the highest activity in photodegradation of phenol. Disregarding the adsorption, the photocatalytic degradation of phenol was fitted well by first-order kinetics with the Langmuir–Hinshelwood mechanism.[1,64] The apparent-reaction-rate constants of phenol degradation on CN, CN-CS-135-3h, CN-CS-150-3h, and CN-CS-180-3h were evaluated as 2.46×10^{-3} (R^2 = 0.994), 2.62×10^{-3} (R^2 = 0.961), 9.84×10^{-3} (R^2 = 0.957), and 11.78×10^{-3} (R^2 = 0.981) min^{-1}, respectively. The reaction rate of CN-CS-180-3h was 4.79 times higher than that of the pristine CN, demonstrating a novel way for improving the photocatalytic oxidation ability of carbon nitride.

Figure 8C shows the effect of hydrothermal time of CN-CS on the photodegradation of phenol solutions. Phenol removal by adsorption was 14.9% in 300 min on CN-CS-150-3h. The photodegradation rates on samples with durations of 1.5 and 6 h were similar, while the sample via the duration of 3 h exhibited the highest activity. As shown in Figure 8D, the 3 h hydrothermal treatment also produced the best catalyst at 180 °C. Sevilla and Fuertes[47] suggested that the duration would significantly affect the diameter and yield of carbon spheres. The lower activities of the samples in hydrothermal treatment for 6 h were possibly due to too much loading of carbon spheres and higher particle size (Figure S4, Supporting Information), which blocks the light absorption.[67] The BET surface area and pore size of CN-CS-180-6h were the lowest among the samples, which might also induce the much lower photocatalytic activity in degradation of phenol.

Figure 9 shows the catalytic stability of the photocatalyst (CN-CS-180) in repeated uses. It was found that, in three runs, the photocatalytic activities did not significantly decrease, indicating a stable performance of the material in photodegradation of organic pollutants.

EPR spectra were applied to identify the reactive species produced by the photocatalyst under irradiation. Figure 10 displays the EPR spectra obtained under dark and irradiation. It

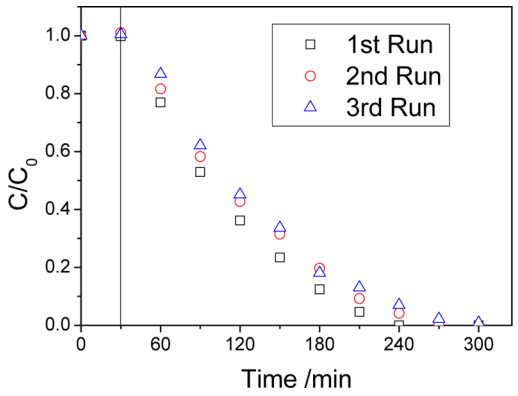

Figure 9. Photocatalytic stability of CN-CS-180 in photodegradation of phenol.

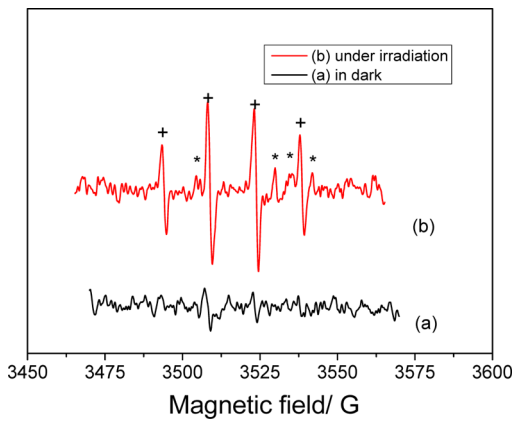

Figure 10. EPR spectra of reactive radicals produced under irradiations; (+) hydroxyl radicals and (*) superoxide radicals.

was found that, under dark, no signals were captured by EPR with the assistance of DMPO in the mixed solution with the

dx.doi.org/10.1021/am503820h | ACS Appl. Mater. Interfaces 2014, 6, 16745−16754

photocatalyst of CN-CS-180-3h, DMPO and phenol. When the suspension was irradiated by UV−visible light, the signals of spin-trapped DMPO−OH· were clearly observed.[68] Moreover, superoxide radicals ($\cdot O_2^-$) were also detected.[69] The EPR studies strongly indicated that the reactive radicals were produced by activation of the photocatalyst under irradiation and that no radicals were generated under dark. The produced radicals have been well-recognized to be responsible for the degradation of organics.

Carbon spheres are widely used as a support and template for hybrid materials or novel nanoarchitectures.[47,51,62] The enhanced photocatalytic oxidation by modification of carbon spheres has not been well explored. Hu et al.[70] reported that coating CdS on colloidal carbon spheres (C@CdS core−shell spheres) can significantly enhance the photodegradation of rhodamine B of CdS nanospheres. The enhanced activity was ascribed to the surface sensitizer of carbonaceous species, and the hydroxyl groups accepting photogenerated holes. Zhou et al.[71] discussed the origin of the enhanced activity of carbon sphere supported Cu_2O catalysts in degradation of methyl orange (MO). The carbon sphere supports were suggested to help adsorb MO reactant and accept electrons from Cu_2O for a better separation rate of photoinduced carries. In this study, the hydrothermal carbonization process would significantly modify g-C_3N_4. First, as evidenced by XRD and SEM, hydrothermal treatment can change the crystal- and microstructure of bulk g-C_3N_4. Second, the intermediates from the aromatization and carbonization can modify the surface properties of pristine g-C_3N_4 and then increase the adsorption of phenol. Third, the formation of carbonaceous materials would improve the visible light absorption by functionalizing as dye sensitization,[33] then increasing the photocatalytic activity. Moreover, the produced intermediates can also serve as a monomer for band gap structure engineering for the enhanced photooxidation.[31,41] As shown in Figure 6, the hydrothermal carbonization at 180 °C can significantly improve the visible light absorption. Meanwhile, hydrothermal treatment at low temperature induces blue-shift. Finally, as shown in SEM/TEM images, stable connections between g-C_3N_4 and carbon nanospheres were formed by the hydrothermal treatment. PL spectra also proved that the separation rate of photogenerated electron/hole pairs was increased, possibly due to the formation of the interfaces between g-C_3N_4 and carbon nanospheres.[67] The higher adsorption of phenol and the higher charge separation rate are more important than the visible light absorption, as evidenced by the results that CN-CS-150 experienced blue-shift but had activity similar to that of CN-CS-180.

4. CONCLUSIONS

Carbon spheres prepared by hydrothermal carbonization of glucose and the structural modification of graphitic carbon nitride were demonstrated to be very effective for improving the photocatalytic activity in oxidation of phenol solutions. The CN-CS sample prepared at 180 °C for 3 h showed activity 4.79 times higher than that of the pristine CN. For the first time, we experimentally proved that crystal- and microstructure, optical property and chemical composition of CN can be significantly modified via the hydrothermal treatment with glucose. As a result, the adsorption of substrate, visible light absorption, and charge transfer in the photodegradation of phenol are thoroughly manipulated, leading to a higher photocatalytic oxidation efficiency. This study therefore provides a new metal-free material for the remediation of organic pollutants and extends the concept of nanomaterials design for a better performance.

■ ASSOCIATED CONTENT

Supporting Information

XRD patterns, N_2 sorption isotherms, FTIR spectra, SEM images, and UV−vis spectra of samples from different hydrothermal conditions. This material is available free of charge via the Internet at http://pubs.acs.org.

■ AUTHOR INFORMATION

Corresponding Authors

*E-mail: shaobin.wang@curtin.edu.au. Tel: +61 8 92663776.
*E-mail: h.sun@curtin.edu.au.

Notes

The authors declare no competing financial interest.

■ ACKNOWLEDGMENTS

This work was financially supported by the Australian Research Council (DP130101319). The authors acknowledge the use of equipment and scientific and technical assistance of the Curtin University Electron Microscope Facility and Centre for Microscopy Characterization and Analysis at the University of Western Australia, which have been partially funded by the University and by State and Commonwealth Governments. H.S. thanks Curtin Research Fellowship and Opening Project (KL13-02) of State Key Laboratory of Materials-Oriented Chemical Engineering, China.

■ REFERENCES

(1) Sun, H. Q.; Ullah, R.; Chong, S. H.; Ang, H. M.; Tade, M. O.; Wang, S. B. Room-Light-Induced Indoor Air Purification Using an Efficient Pt/N-TiO_2 Photocatalyst. *Appl. Catal., B* **2011**, *108*, 127−133.

(2) Sun, H. Q.; Bai, Y.; Liu, H. J.; Jin, W. Q.; Xu, N. P.; Chen, G. J.; Xu, B. Q. Mechanism of Nitrogen-Concentration Dependence on pH Value: Experimental and Theoretical Studies on Nitrogen-Doped TiO_2. *J. Phys. Chem. C* **2008**, *112*, 13304−13309.

(3) Sun, H.; Liu, S.; Liu, S.; Wang, S. A Comparative Study of Reduced Graphene Oxide Modified TiO_2, ZnO, and Ta_2O_5 in Visible Light Photocatalytic/Photochemical Oxidation of Methylene Blue. *Appl. Catal., B* **2014**, *146*, 162−168.

(4) Khan, Z.; Chetia, T. R.; Qureshi, M. Rational Design of Hyperbranched 3D Heteroarrays of SrS/CdS: Synthesis, Characterization and Evaluation of Photocatalytic Properties for Efficient Hydrogen Generation and Organic Dye Degradation. *Nanoscale* **2012**, *4*, 3543−3550.

(5) Xiong, Z. G.; Zhang, L. L.; Ma, J. Z.; Zhao, X. S. Photocatalytic Degradation of Dyes over Graphene−Gold Nanocomposites under Visible Light Irradiation. *Chem. Commun.* **2010**, *46*, 6099−6101.

(6) Zhang, J.; Liu, X.; Blume, R.; Zhang, A. H.; Schlogl, R.; Su, D. S. Surface-Modified Carbon Nanotubes Catalyze Oxidative Dehydrogenation of n-Butane. *Science* **2008**, *322*, 73−77.

(7) Liu, L.; Deng, Q. F.; Agula, B.; Zhao, X.; Ren, T. Z.; Yuan, Z. Y. Ordered Mesoporous Carbon Catalyst for Dehydrogenation of Propane to Propylene. *Chem. Commun.* **2011**, *47*, 8334−8336.

(8) Silva, R.; Voiry, D.; Chhowalla, M.; Asefa, T. Efficient Metal-Free Electrocatalysts for Oxygen Reduction: Polyaniline-Derived N- and O-Doped Mesoporous Carbons. *J. Am. Chem. Soc.* **2013**, *135*, 7823−7826.

(9) Ju, M. J.; Kim, J. C.; Choi, H. J.; Choi, I. T.; Kim, S. G.; Lim, K.; Ko, J.; Lee, J. J.; Jeon, I. Y.; Baek, J. B.; Kim, H. K. N-Doped Graphene Nanoplatelets as Superior Metal-Free Counter Electrodes for Organic Dye-Sensitized Solar Cells. *ACS Nano* **2013**, *7*, 5243−5250.

(10) Peng, W. C.; Liu, S. Z.; Sun, H. Q.; Yao, Y. J.; Zhi, L. J.; Wang, S. B. Synthesis of Porous Reduced Graphene Oxide as Metal-Free Carbon for Adsorption and Catalytic Oxidation of Organics in Water. *J. Mater. Chem. A* **2013**, *1*, 5854−5859.
(11) Sun, H. Q.; Liu, S. Z.; Zhou, G. L.; Ang, H. M.; Tade, M. O.; Wang, S. B. Reduced Graphene Oxide for Catalytic Oxidation of Aqueous Organic Pollutants. *ACS Appl. Mater. Interfaces* **2012**, *4*, 5466−5471.
(12) Sun, H. Q.; Wang, Y. X.; Liu, S. Z.; Ge, L.; Wang, L.; Zhu, Z. H.; Wang, S. B. Facile Synthesis of Nitrogen Doped Reduced Graphene Oxide as a Superior Metal-Free Catalyst for Oxidation. *Chem. Commun.* **2013**, *49*, 9914−9916.
(13) Sun, H. Q.; Liang, H. W.; Zhou, G. L.; Wang, S. B. Supported Cobalt Catalysts by One-Pot Aqueous Combustion Synthesis for Catalytic Phenol Degradation. *J. Colloid Interface Sci.* **2013**, *394*, 394−400.
(14) Saputra, E.; Muhammad, S.; Sun, H. Q.; Ang, H. M.; Tade, M. O.; Wang, S. B. Different Crystallographic One-Dimensional MnO_2 Nanomaterials and Their Superior Performance in Catalytic Phenol Degradation. *Environ. Sci. Technol.* **2013**, *47*, 5882−5887.
(15) Hsu, H. C.; Shown, I.; Wei, H. Y.; Chang, Y. C.; Du, H. Y.; Lin, Y. G.; Tseng, C. A.; Wang, C. H.; Chen, L. C.; Lin, Y. C.; Chen, K. H. Graphene Oxide as a Promising Photocatalyst for CO_2 to Methanol Conversion. *Nanoscale* **2013**, *5*, 262−268.
(16) Zhang, L. L.; Xiong, Z. G.; Zhao, X. S. Pillaring Chemically Exfoliated Graphene Oxide with Carbon Nanotubes for Photocatalytic Degradation of Dyes under Visible Light Irradiation. *ACS Nano* **2010**, *4*, 7030−7036.
(17) Li, H. T.; Liu, R. H.; Lian, S. Y.; Liu, Y.; Huang, H.; Kang, Z. H. Near-Infrared Light Controlled Photocatalytic Activity of Carbon Quantum Dots for Highly Selective Oxidation Reaction. *Nanoscale* **2013**, *5*, 3289−3297.
(18) Liu, J. K.; Wen, S. H.; Hou, Y.; Zuo, F.; Beran, G. J. O.; Feng, P. Y. Boron Carbides as Efficient, Metal-Free, Visible-Light-Responsive Photocatalysts. *Angew. Chem., Int. Ed.* **2013**, *52*, 3241−3245.
(19) Liu, G.; Niu, P.; Yin, L. C.; Cheng, H. M. α-Sulfur Crystals as a Visible-Light-Active Photocatalyst. *J. Am. Chem. Soc.* **2012**, *134*, 9070−9073.
(20) Wang, F.; Ng, W. K. H.; Yu, J. C.; Zhu, H. J.; Li, C. H.; Zhang, L.; Liu, Z. F.; Li, Q. Red Phosphorus: An Elemental Photocatalyst for Hydrogen Formation from Water. *Appl. Catal., B* **2012**, *111*, 409−414.
(21) Liu, G.; Yin, L. C.; Niu, P.; Jiao, W.; Cheng, H. M. Visible-Light-Responsive β-Rhombohedral Boron Photocatalysts. *Angew. Chem., Int. Ed.* **2013**, *52*, 6242−6245.
(22) Wang, X. C.; Blechert, S.; Antonietti, M. Polymeric Graphitic Carbon Nitride for Heterogeneous Photocatalysis. *ACS Catal.* **2012**, *2*, 1596−1606.
(23) Zheng, Y.; Liu, J.; Liang, J.; Jaroniec, M.; Qiao, S. Z. Graphitic Carbon Nitride Materials: Controllable Synthesis and Applications in Fuel Cells and Photocatalysis. *Energy Environ. Sci.* **2012**, *5*, 6717−6731.
(24) Tahir, M.; Cao, C. B.; Mahmood, N.; Butt, F. K.; Mahmood, A.; Idrees, F.; Hussain, S.; Tanveer, M.; Ali, Z.; Aslam, I. Multifunctional g-C_3N_4 Nanofibers: A Template-Free Fabrication and Enhanced Optical, Electrochemical, and Photocatalyst Properties. *ACS Appl. Mater. Interfaces* **2014**, *6*, 1258−1265.
(25) Wang, X. C.; Maeda, K.; Thomas, A.; Takanabe, K.; Xin, G.; Carlsson, J. M.; Domen, K.; Antonietti, M. A Metal-Free Polymeric Photocatalyst for Hydrogen Production from Water under Visible Light. *Nat. Mater.* **2009**, *8*, 76−80.
(26) Zhang, J. S.; Sun, J. H.; Maeda, K.; Domen, K.; Liu, P.; Antonietti, M.; Fu, X. Z.; Wang, X. C. Sulfur-Mediated Synthesis of Carbon Nitride: Band-Gap Engineering and Improved Functions for Photocatalysis. *Energy Environ. Sci.* **2011**, *4*, 675−678.
(27) Yan, H. J. Soft-Templating Synthesis of Mesoporous Graphitic Carbon Nitride with Enhanced Photocatalytic H_2 Evolution under Visible Light. *Chem. Commun.* **2012**, *48*, 3430−3432.
(28) Liu, J.; Huang, J. H.; Zhou, H.; Antonietti, M. Uniform Graphitic Carbon Nitride Nanorod for Efficient Photocatalytic Hydrogen Evolution and Sustained Photoenzymatic Catalysis. *ACS Appl. Mater. Interfaces* **2014**, *6*, 8434−8440.
(29) Zhang, Y. W.; Liu, J. H.; Wu, G.; Chen, W. Porous Graphitic Carbon Nitride Synthesized via Direct Polymerization of Urea for Efficient Sunlight-Driven Photocatalytic Hydrogen Production. *Nanoscale* **2012**, *4*, 5300−5303.
(30) Wang, Y. J.; Shi, R.; Lin, J.; Zhu, Y. F. Enhancement of Photocurrent and Photocatalytic Activity of ZnO Hybridized with Graphite-Like C_3N_4. *Energy Environ. Sci.* **2011**, *4*, 2922−2929.
(31) Chu, S.; Wang, Y.; Guo, Y.; Feng, J. Y.; Wang, C. C.; Luo, W. J.; Fan, X. X.; Zou, Z. G. Band Structure Engineering of Carbon Nitride: In Search of a Polymer Photocatalyst with High Photooxidation Property. *ACS Catal.* **2013**, *3*, 912−919.
(32) Liao, G. Z.; Chen, S.; Quan, X.; Yu, H. T.; Zhao, H. M. Graphene Oxide Modified g-C_3N_4 Hybrid with Enhanced Photocatalytic Capability under Visible Light Irradiation. *J. Mater. Chem.* **2012**, *22*, 2721−2726.
(33) Wang, Y. B.; Hong, J. D.; Zhang, W.; Xu, R. Carbon Nitride Nanosheets for Photocatalytic Hydrogen Evolution: Remarkably Enhanced Activity by Dye Sensitization. *Catal. Sci. Technol.* **2013**, *3*, 1703−1711.
(34) Chen, X. F.; Zhang, J. S.; Fu, X. Z.; Antonietti, M.; Wang, X. C. Fe-g-C_3N_4-Catalyzed Oxidation of Benzene to Phenol Using Hydrogen Peroxide and Visible Light. *J. Am. Chem. Soc.* **2009**, *131*, 11658−11659.
(35) Liu, G.; Niu, P.; Sun, C. H.; Smith, S. C.; Chen, Z. G.; Lu, G. Q.; Cheng, H. M. Unique Electronic Structure Induced High Photoreactivity of Sulfur-Doped Graphitic C_3N_4. *J. Am. Chem. Soc.* **2010**, *132*, 11642−11648.
(36) Sun, H. Q.; Wang, S. B. Research Advances in the Synthesis of Nanocarbon-Based Photocatalysts and Their Applications for Photocatalytic Conversion of Carbon Dioxide to Hydrocarbon Fuels. *Energy Fuels* **2014**, *28*, 22−36.
(37) Zhang, J. S.; Chen, X. F.; Takanabe, K.; Maeda, K.; Domen, K.; Epping, J. D.; Fu, X. Z.; Antonietti, M.; Wang, X. C. Synthesis of a Carbon Nitride Structure for Visible-Light Catalysis by Copolymerization. *Angew. Chem., Int. Ed.* **2010**, *49*, 441−444.
(38) Niu, P.; Zhang, L. L.; Liu, G.; Cheng, H. M. Graphene-Like Carbon Nitride Nanosheets for Improved Photocatalytic Activities. *Adv. Funct. Mater.* **2012**, *22*, 4763−4770.
(39) Mao, J.; Peng, T. Y.; Zhang, X. H.; Li, K.; Ye, L. Q.; Zan, L. Effect of Graphitic Carbon Nitride Microstructures on the Activity and Selectivity of Photocatalytic CO_2 Reduction under Visible Light. *Catal. Sci. Technol.* **2013**, *3*, 1253−1260.
(40) Han, K. K.; Wang, C. C.; Li, Y. Y.; Wan, M. M.; Wang, Y.; Zhu, J. H. Facile Template-Free Synthesis of Porous g-C_3N_4 with High Photocatalytic Performance under Visible Light. *RSC Adv.* **2013**, *3*, 9465−9469.
(41) Shalom, M.; Inal, S.; Fettkenhauer, C.; Neher, D.; Antonietti, M. Improving Carbon Nitride Photocatalysis by Supramolecular Preorganization of Monomers. *J. Am. Chem. Soc.* **2013**, *135*, 7118−7121.
(42) Lee, S. C.; Lintang, H. O.; Yuliati, L. A Urea Precursor to Synthesize Carbon Nitride with Mesoporosity for Enhanced Activity in the Photocatalytic Removal of Phenol. *Chem.—Asian J.* **2012**, *7*, 2139−2144.
(43) Cui, Y. J.; Huang, J. H.; Fu, X. Z.; Wang, X. C. Metal-Free Photocatalytic Degradation of 4-Chlorophenol in Water by Mesoporous Carbon Nitride Semiconductors. *Catal. Sci. Technol.* **2012**, *2*, 1396−1402.
(44) Chang, C.; Zhu, L. Y.; Wang, S. F.; Chu, X. L.; Yue, L. F. Novel Mesoporous Graphite Carbon Nitride/BiOI Heterojunction for Enhancing Photocatalytic Performance Under Visible-Light Irradiation. *ACS Appl. Mater. Interfaces* **2014**, *6*, 5083−5093.
(45) Wang, Q.; Li, H.; Chen, L. Q.; Huang, X. J. Monodispersed Hard Carbon Spherules with Uniform Nanopores. *Carbon* **2001**, *39*, 2211−2214.
(46) Yu, S. H.; Cui, X. J.; Li, L. L.; Li, K.; Yu, B.; Antonietti, M.; Colfen, H. From Starch to Metal/Carbon Hybrid Nanostructures:

Hydrothermal Metal-Catalyzed Carbonization. *Adv. Mater.* **2004**, *16*, 1636−1637.
(47) Sevilla, M.; Fuertes, A. B. Chemical and Structural Properties of Carbonaceous Products Obtained by Hydrothermal Carbonization of Saccharides. *Chem.—Eur. J.* **2009**, *15*, 4195−4203.
(48) Yao, C.; Shin, Y.; Wang, L. Q.; Windisch, C. F.; Samuels, W. D.; Arey, B. W.; Wang, C.; Risen, W. M.; Exarhos, G. J. Hydrothermal Dehydration of Aqueous Fructose Solutions in a Closed System. *J. Phys. Chem. C* **2007**, *111*, 15141−15145.
(49) Zheng, M. T.; Liu, Y. L.; Xiao, Y.; Zhu, Y.; Guan, Q.; Yuan, D. S.; Zhang, J. X. An Easy Catalyst-Free Hydrothermal Method to Prepare Monodisperse Carbon Microspheres on a Large Scale. *J. Phys. Chem. C* **2009**, *113*, 8455−8459.
(50) Yan, S. C.; Li, Z. S.; Zou, Z. G. Photodegradation Performance of g-C_3N_4 Fabricated by Directly Heating Melamine. *Langmuir* **2009**, *25*, 10397−10401.
(51) Sun, H. Q.; Zhou, G. L.; Liu, S. Z.; Ang, H. M.; Tade, M. O.; Wang, S. B. Nano-Fe^0 Encapsulated in Microcarbon Spheres: Synthesis, Characterization, and Environmental Applications. *ACS Appl. Mater. Interfaces* **2012**, *4*, 6235−6241.
(52) Bai, X. J.; Wang, L.; Zong, R. L.; Zhu, Y. F. Photocatalytic Activity Enhanced via g-C_3N_4 Nanoplates to Nanorods. *J. Phys. Chem. C* **2013**, *117*, 9952−9961.
(53) Groenewolt, M.; Antonietti, M. Synthesis of g-C_3N_4 Nanoparticles in Mesoporous Silica Host Matrices. *Adv. Mater.* **2005**, *17* (14), 1789−1790.
(54) Goettmann, F.; Fischer, A.; Antonietti, M.; Thomas, A. Chemical Synthesis of Mesoporous Carbon Nitrides using Hard Templates and Their Use as a Metal-Free Catalyst for Friedel−Crafts Reaction of Benzene. *Angew. Chem., Int. Ed.* **2006**, *45*, 4467−4471.
(55) Sano, T.; Tsutsui, S.; Koike, K.; Hirakawa, T.; Teramoto, Y.; Negishi, N.; Takeuchi, K. Activation of Graphitic Carbon Nitride (g-C_3N_4) by Alkaline Hydrothermal Treatment for Photocatalytic NO Oxidation in Gas Phase. *J. Mater. Chem. A* **2013**, *1*, 6489−6496.
(56) Zhang, G. G.; Zhang, J. S.; Zhang, M. W.; Wang, X. C. Polycondensation of Thiourea into Carbon Nitride Semiconductors as Visible Light Photocatalysts. *J. Mater. Chem.* **2012**, *22*, 8083−8091.
(57) Xin, G.; Meng, Y. L. Pyrolysis Synthesized g-C_3N_4 for Photocatalytic Degradation of Methylene Blue. *J. Chem.* **2013**, DOI: 10.1155/2013/187912.
(58) Lotsch, B. V.; Doblinger, M.; Sehnert, J.; Seyfarth, L.; Senker, J.; Oeckler, O.; Schnick, W. Unmasking Melon by a Complementary Approach Employing Electron Diffraction, Solid-State NMR Spectroscopy, and Theoretical Calculations-Structural Characterization of a Carbon Nitride Polymer. *Chem.—Eur. J.* **2007**, *13*, 4969−4980.
(59) Demir-Cakan, R.; Baccile, N.; Antonietti, M.; Titirici, M. M. Carboxylate-Rich Carbonaceous Materials via One-Step Hydrothermal Carbonization of Glucose in the Presence of Acrylic Acid. *Chem. Mater.* **2009**, *21*, 484−490.
(60) Chen, C. Y.; Sun, X. D.; Jiang, X. C.; Niu, D.; Yu, A. B.; Liu, Z. G.; Li, J. G. A Two-Step Hydrothermal Synthesis Approach to Monodispersed Colloidal Carbon Spheres. *Nanoscale Res. Lett.* **2009**, *4*, 971−976.
(61) Li, J. H.; Shen, B. A.; Hong, Z. H.; Lin, B. Z.; Gao, B. F.; Chen, Y. L. A Facile Approach to Synthesize Novel Oxygen-Doped g-C_3N_4 with Superior Visible-Light Photoreactivity. *Chem. Commun.* **2012**, *48*, 12017−12019.
(62) Sun, X. M.; Li, Y. D. Colloidal Carbon Spheres and Their Core/Shell Structures with Noble-Metal Nanoparticles. *Angew. Chem., Int. Ed.* **2004**, *43*, 597−601.
(63) Zhang, Y. J.; Thomas, A.; Antonietti, M.; Wang, X. C. Activation of Carbon Nitride Solids by Protonation: Morphology Changes, Enhanced Ionic Conductivity, and Photoconduction Experiments. *J. Am. Chem. Soc.* **2009**, *131*, 50−51.
(64) Sun, H.; Zhou, G.; Liu, S.; Ang, H. M.; Tadé, M. O.; Wang, S. Visible Light Responsive Titania Photocatalysts Codoped by Nitrogen and Metal (Fe, Ni, Ag, or Pt) for Remediation of Aqueous Pollutants. *Chem. Eng. J.* **2013**, *231*, 18−25.
(65) Ge, L.; Han, C. C.; Liu, J. In Situ Synthesis and Enhanced Visible Light Photocatalytic Activities of Novel PANI-g-C_3N_4 Composite Photocatalysts. *J. Mater. Chem.* **2012**, *22*, 11843−11850.
(66) He, F.; Chen, G.; Yu, Y. G.; Hao, S.; Zhou, Y. S.; Zheng, Y. Facile Approach to Synthesize g-PAN/g-C_3N_4 Composites with Enhanced Photocatalytic H_2 Evolution Activity. *ACS Appl. Mater. Interfaces* **2014**, *6*, 7171−7179.
(67) Liu, S. Z.; Sun, H. Q.; Liu, S. M.; Wang, S. B. Graphene Facilitated Visible Light Photodegradation of Methylene Blue over Titanium Dioxide Photocatalysts. *Chem. Eng. J.* **2013**, *214*, 298−303.
(68) Qiu, R. L.; Zhang, D. D.; Mo, Y. Q.; Song, L.; Brewer, E.; Huang, X. F.; Xiong, Y. Photocatalytic Activity of Polymer-Modified ZnO under Visible Light Irradiation. *J. Hazard. Mater.* **2008**, *156*, 80−85.
(69) Han, C. C.; Ge, L.; Chen, C. F.; Li, Y. J.; Xiao, X. L.; Zhang, Y. N.; Guo, L. L. Novel Visible Light Induced Co_3O_4-g-C_3N_4 Heterojunction Photocatalysts for Efficient Degradation of Methyl Orange. *Appl. Catal., B* **2014**, *147*, 546−553.
(70) Hu, Y.; Liu, Y.; Qian, H. S.; Li, Z. Q.; Chen, J. F. Coating Colloidal Carbon Spheres with CdS Nanoparticles: Microwave-Assisted Synthesis and Enhanced Photocatalytic Activity. *Langmuir* **2010**, *26*, 18570−18575.
(71) Zhou, K. Q.; Shi, Y. Q.; Jiang, S. H.; Hu, Y.; Gui, Z. Facile Preparation of Cu_2O/Carbon Sphere Heterostructure with High Photocatalytic Activity. *Mater. Lett.* **2013**, *98*, 213−216.